

Model-Free and Real-Time Bioinspired Unicycle-Based Source Seeking: Differential Wheeled Robotic Experiments

Ahmed A. Elgohary

PhD Student

Department of Aerospace Engineering and Engineering Mechanics,
University of Cincinnati, OH, USA

Sameh A. Eisa

Assistant Professor

Department of Aerospace Engineering and Engineering Mechanics,
University of Cincinnati, OH, USA

Shivam Bajpai

MS Student

Department of Aerospace Engineering and Engineering Mechanics,
University of Cincinnati, OH, USA

Abstract. Bioinspired robots aimed at source-seeking are often studied, and their controls designed, using unicycle modeling and formulation. This is true not only for model-based controllers, but also for model-free, real-time control methods such as extremum seeking control (ESC). In this paper, we propose a unicycle-based ESC design applicable to differential wheeled robots that: (1) is very simple design, based on one simple control-affine law, and without state integrators; (2) attenuates oscillations known to persist in ESC designs (i.e., fully stop at the source); and (3) operates in a model-free, real-time setting, tolerating environmental/sensor noise. We provide simulation and real-world robotic experimental results for fixed and moving light source seeking by a differential wheeled robot using our proposed design. Results indicate clear advantages of our proposed design when compared to the literature, including attenuation of undesired oscillations, improved convergence speed, and better handling of noise.

1. Introduction

The problem of source-seeking by robots has been extensively studied due to its importance in various applications, including environmental monitoring, chemical plume tracking, and search-and-rescue missions [1–3], among others. To elaborate further, the source-seeking problem is usually understood as studying/proposing a control method, technique and/or design, which aims at steering autonomously a system (usually

unmanned, mobile robot) towards the source, which represents the maximum/minimum intensity of a physical field (scalar signal such as heat, light, or chemical concentration, among others), using on-board sensors. Over the years, numerous control strategies have been developed to address the source-seeking problem. For instance, proportional-integral-derivative (PID) controllers and model predictive controllers (MPC), have been widely employed [4–9]. While these approaches can be promising, they often require accurate mathematical models of the system and the environment, which may not always be available or practical. In contrast, recent advancements have explored model-free, real-time extremum seeking approaches (including some experimental work) [10–18], which eliminate the need for detailed system models and can adapt to uncertainties and dynamic environments (i.e., more practical). Figure 1 depicts the basic idea behind the source-seeking problem (especially in the context of extremum seeking approaches). It is assumed that the physical field (scalar signal) is unknown – expression wise. The robot controller is designed to steer the robot, using only the sensor local information, to the source of said unknown scalar signal.

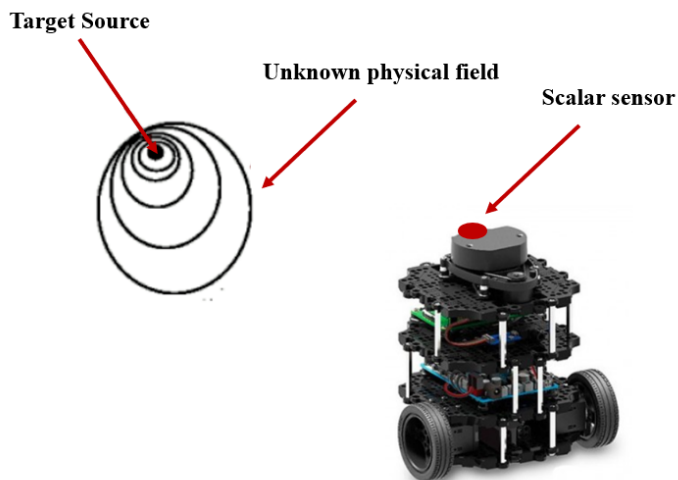


Figure 1: Source-seeking based on sensor measurements for a differential wheeled robot.

It is observed in nature that many organisms conduct source-seeking (and/or trajectory tracking) behaviors for various objectives, such as catching a prey, moving towards a heat/light source, or locating a chemical trail. These organisms often achieve model-free (presumably), real-time dynamic optimization and control in an efficient manner, relying only on their sensations. For example, sharks detect gradients in electric fields to locate prey [19], snakes use thermal sensing to detect warm-blooded animals even in complete darkness [20], and albatrosses use their nostrils as a wind speed sensor [21] to guide for minimal flight effort. Inspired by these natural phenomena and many others in nature, researchers have sought to emulate nature’s strategies in solving the source-seeking problem depicted in Figure 1. By studying dynamic optimization methods and source-seeking in biological systems, researchers aimed at developing bio-

inspired robots that act more like natural organisms in efficiency and objectives, see for example [6, 22–27]. It is also worth mentioning that in many bio-inspired robotic works for source-seeking [6, 18, 23, 24], the simple unicycle model (will be discussed in Section 2.1) is often used to represent the robot dynamics and facilitate control design. This approach is particularly useful for differential wheeled robots as they operate naturally and effectively using unicycle designs [6, 18, 23, 24] as will be shown in Section 2.1.

In this paper, we focus on addressing the source-seeking problem through a bio-inspired approach grounded in extremum seeking control (ESC), as illustrated in Figure 2. ESC methods are particularly appealing due to their model-free nature, stability, robustness against uncertainties, and real-time operability [28–30]. These characteristics make them an ideal choice for capturing and mimicking the source-seeking and dynamic optimization behaviors observed in nature, and consequently, bio-inspired source-seeking by robots. As shown in Figure 2, ESC has a natural ability to emulate the dynamic decision-making processes in biological systems. For instance, it has been successfully applied to the dynamic soaring problem of soaring birds like albatrosses, showcasing its ability to optimize energy-efficient trajectories in uncertain wind environments [31, 32]. Similarly, ESC has been employed to study and emulate hovering in flapping insects and hummingbirds [33]. It has also been used in formation flight scenarios [34]. Additionally, ESC has been successfully used to emulate source-seeking of the egg by sperm [35], source-seeking by bacteria [36] and source-seeking by fish [11].

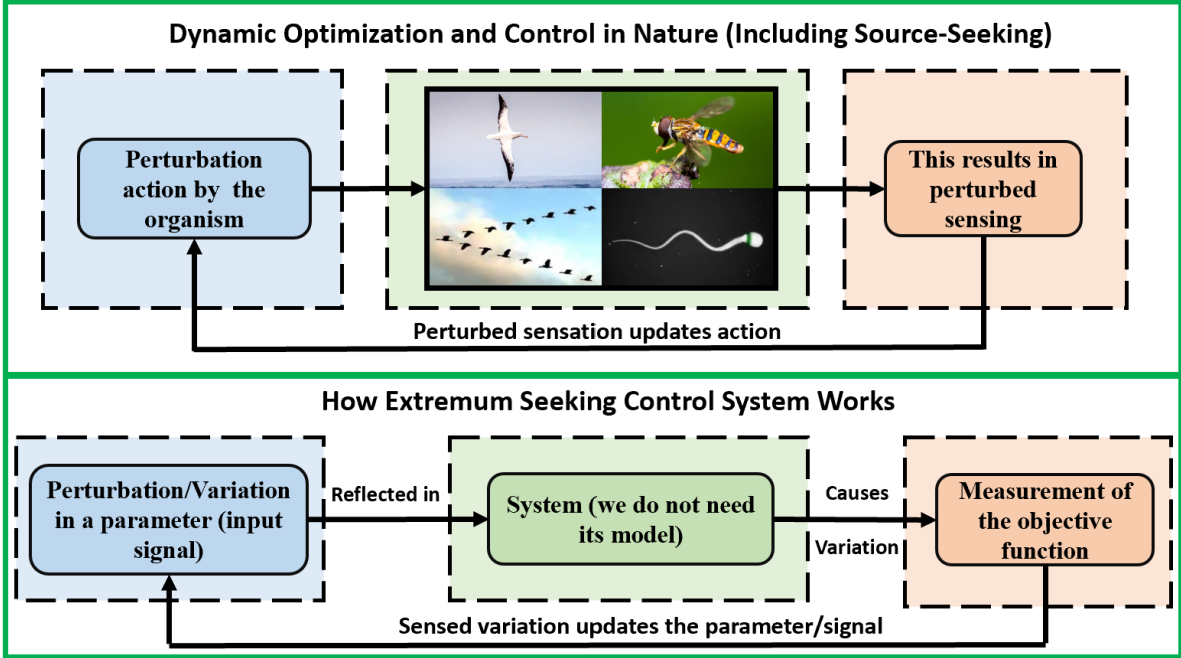


Figure 2: Parallelism has been observed in recent literature between ESC (lower part), and many dynamic optimization and source-seeking behaviors in nature (upper part) [11, 31–36]. Hence, source-seeking by robots using ESC is a bio-inspired approach.

1.1. Motivation

ESC is a promising solution for the source-seeking problem in Figure 1, especially for how it emulates nature’s optimization and source-seeking strategies very effectively (Figure 2). Source-seeking via ESC will only need local measurements (via sensors) of the scalar signal (e.g., light), without any need for the mathematical model of the robot or the mathematical expression of the physical environment, presumably, similar to how very simple organisms in nature conduct source-seeking. However, for real-world deployments, involving ESC in robotics often encounters challenges due to the continuous oscillations inherited generally in the ESC control inputs (e.g., linear and angular velocities in robots) [37–39]. This also leads to persistent oscillations about the source (the extremum point for which the ESC converges to). While these oscillations in the control inputs are generally manageable and do not hinder the feasibility of real-world source-seeking experiments involving ESC (e.g., [40–43]), they can limit performance in terms of convergence speed and precision near the extremum (i.e., the source). Also, persistent oscillations mean that the system (e.g., robot) will not automatically stop at the source or slow down its oscillations as the system gets closer to the source. We observed these limitations in a prior work [44] using a differential wheeled robot, namely Turtlebot3 [45], which aimed at replicating the classical ESC-based source seeking approach in [40] – see our YouTube video in [46].

For the focus of this paper, we turn our attention to control-affine ESC structures [38, 39, 47, 48] that are very natural to robotic applications; for example, the unicycle representation of robotics can be considered directly a control-affine ESC (e.g. [38]). Moreover, some control-affine ESC structures offer simplicity in design, reduced parameter tuning, and guaranteed stability under certain conditions [38, 39, 47, 48]. Particularly, the control-affine ESC law in (1) is very simple:

$$\dot{x} = u = f(x)u_1 + u_2, \quad (1)$$

where x is the variable (e.g., x -coordinate of the robot) controlled by the law u involving $f(x)$, which is the unknown objective function (e.g., the scalar signal in the source-seeking problem), and u_1, u_2 are perturbation/excitation signals (e.g., sinusoidal signals). As known in the ESC literature [38, 39, 47, 48], the control law in (1) approximates a gradient flow, without access to the formula of the objective function $f(x)$ or its gradient, which dynamically updates x to derive the system to the extremum of $f(x)$ (e.g., the source). However, real-world robotic deployments for control-affine ESC are rare and fall short. Experimental results in [13] identified the simple control-affine ESC law in (1) to have the weakest performance in their robotic experiments. Furthermore, theoretical analyses in [48] demonstrated that control-affine ESC systems in the form of (1) by themselves lack the ability to attenuate oscillations as they approach the extremum and cannot achieve asymptotic convergence, instead oscillating indefinitely around the target/source. Recently [12], we were able to overcome all mentioned limitations and demonstrate in light source-seeking robotic experiments the ability of the

simple control-affine ESC law in (1) to perform model-free, real-time source-seeking and with attenuating oscillations – thanks to our recent theoretical results in [49] and the new ESC class therein. However, we did not provide source-seeking robotic experiments using the unicycle representation of robots, which is clearly the most efficient and commonly used representation, especially in bio-inspired robotics [6, 18, 23, 24].

1.2. Contribution and organization of the paper

In this paper, we provide a design and real-world robotic experiments of a newly proposed unicycle-based ESC aimed at performing model-free, real-time source-seeking. The following points highlight the contributions provided in this paper:

- We adopt unicycle control-affine design, often representing bio-inspired robotics (e.g., [6, 18, 23, 24]) based only on one simple ESC control law (1) and show its effectiveness in model-free, real-time light source-seeking experiments.
- For the first time in literature, we provide a design followed by robotic experimental results that enable *unicycle-based ESC with attenuating oscillations based on the very simple control law* (1). That is, the robot reduces oscillations as it approaches the extremum (the source). As a result, we are able to provide an algorithm, which stops the robot at the source instead of keeping it persistently oscillating. It is important to emphasize that this novel real-world deployment is based on, and verifies further, our recent theoretical results in [49] and the applicability of the ESC class therein (control-affine ESC systems that attenuate oscillations structurally). We verified [49] experimentally before in [12] for single-integrator-based ESC, not unicycle-based ESC; the latter will be proven much more effective as will be discussed in Section 4.4.
- For the first time in literature, the recently developed Geometric-based Extended Kalman Filter (GEKF) [50] is tested successfully in real-world experiment with unicycle-based ESC design. In fact, the use of GEKF, not only was necessary for attenuating undesired oscillations, it also improved the convergence of our unicycle-based ESC *significantly* even in a noisy environment (i.e., GEKF was proven to improve the handling of noise due to the use of sensor).
- In our experiments, we used a differential wheeled robot [45] as these kinds of robots are very natural to bio-inspired unicycle source-seeking [6, 18, 23, 24]. One huge advantage is that the use of the ESC law in (1) with differential wheeled robots, means we achieve a very simple design with no state integrators at all, unlike traditional control-affine ESC designs [37–39]. That is, the proposed bio-inspired unicycle-based ESC is far less complex than the simple single-integrator-based ESC design we proposed and experimented in [12], and with much higher efficiency and practical relevance.

In summary, the proposed design is a very simple, model-free, real-time design that: (i) has no state integrators; (ii) has attenuating oscillations, enabling the robot to stop

at the source; (iii) has improved convergence speed; and (IV) handles noise better. In Section 2, we provide background and information on unicycle representation of robots, relevant ESC structure, and GEKF. In Section 3, we provide the proposed unicycle-based ESC design, the implementation algorithm, and the advantages of proposed design compared to literature. In Section 4, we provide simulations, real-world experimental results with known objective function to test the proposed design, and model-free real-world experiments of light source seeking. We conclude the paper in Section 5.

2. Background: Unicycle Representation for Robots, Control-affine Extremum Seeking Controllers, and Geometric-based Kalman Filtering

2.1. Unicycle Dynamic Model: Effective Representation for Many Robots

The unicycle dynamic model has been applied in numerous robotics and control applications, particularly in source-seeking applications (including bio-inspired ones) – see for example [6, 13, 16–18, 23, 24, 36, 38, 51]. Its simplicity makes it a highly effective representation of robot dynamics, facilitating both analysis and control design. The unicycle model simplifies the representation of robotic motion by considering only a single forward velocity and angular velocity, effectively describing the dynamics of many robotic platforms within a compact and straightforward mathematical framework. For differential wheeled robots, such as but not limited to Turtlebot3 [45], the unicycle model provides a natural and effective abstraction since the dynamics of such robots inherently align with unicycle-like motion. By controlling the linear velocity v and/or the angular velocity ω , differential wheeled robots can perform smooth maneuvers, making the unicycle model an ideal candidate for motion planning, trajectory tracking, and bio-inspired navigation tasks.

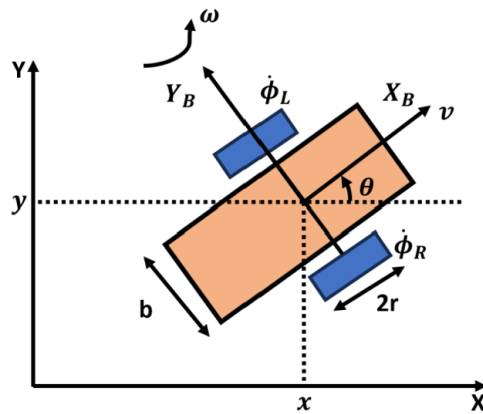


Figure 3: An illustration of a differential wheeled robot (sometimes referred to as differential drive robot).

Figure 3 shows a differential wheeled mobile robot, where the global and body-fixed axes are denoted by (X, Y) and (X_B, Y_B) , respectively. The simple unicycle

representation, which serves as an abstraction for differential wheeled robots, can be expressed as:

$$\begin{aligned}\dot{x} &= v \cos \theta, \\ \dot{y} &= v \sin \theta, \\ \dot{\theta} &= \omega,\end{aligned}\tag{2}$$

where x and y represent the position states of the robot, θ represents its orientation with respect to the horizontal axis, v is the linear velocity, and ω is the angular velocity. Typically, the linear velocity v and angular velocity ω are the control inputs for such robots. In model-based control methods, they are often derived and/or related to the left and right wheel velocities $\dot{\phi}_L$ and $\dot{\phi}_R$, along with the wheel radius r and the wheelbase b to capture more geometric and body details (i.e., to better model the robot for more accurate control design and dynamic simulation). However, in this work, we use ESC for the differential wheeled robot. Hence, the model-free nature of the ESC enables direct control laws for v and/or w without needing details on $\dot{\phi}_L$, $\dot{\phi}_R$, r and b or explicit relationships between them and v or ω .

2.2. Relevant Class of Control-affine Extremum Seeking Controllers

Let us start with the class of control-affine ESC below [38, 39]:

$$\dot{\mathbf{x}} = \mathbf{b}_d(t, \mathbf{x}) + \sum_{i=1}^m \mathbf{b}_i(t, \mathbf{x}) \sqrt{\omega} u_i(\omega t),\tag{3}$$

where $\mathbf{x} \in \mathbb{R}^n$ is the state space vector, \mathbf{b}_d is the drift vector field (uncontrolled dynamics), m is the number of control inputs, u_i are the control inputs, \mathbf{b}_i are the control vector fields, and $\omega \in (0, \infty)$ is a frequency parameter. Control-affine ESC systems in the form of (3) can be approximated by what is known as Lie Bracket System (LBS) [39]. In other words, the trajectory of a control-affine ESC system can be approximated by the trajectory of the corresponding LBS. In fact, very recently, we have been able to prove that LBS approximations to control-affine systems (including ESC) are, in fact, higher-order averaging themselves, i.e. they follow the traditional averaging analysis [39]. Now, the control-affine ESC system in (3) can be approximated and represented by the LBS [38, 39]:

$$\dot{\mathbf{z}} = \mathbf{b}_d(t, \mathbf{z}) + \sum_{\substack{i=1 \\ j=i+1}}^m [\mathbf{b}_i, \mathbf{b}_j](t, \mathbf{z}) \nu_{j,i}(t),\tag{4}$$

with $\nu_{j,i}(t) = \frac{1}{T} \int_0^T u_j(t, \theta) \int_0^\theta u_i(t, \tau) d\tau d\theta$, and the Lie bracket operation $[\mathbf{b}_i, \mathbf{b}_j]$ is defined as:

$$[\mathbf{b}_i, \mathbf{b}_j](t, \mathbf{x}) := \frac{\partial \mathbf{b}_j(t, \mathbf{x})}{\partial \mathbf{x}} \mathbf{b}_i(t, \mathbf{x}) - \frac{\partial \mathbf{b}_i(t, \mathbf{x})}{\partial \mathbf{x}} \mathbf{b}_j(t, \mathbf{x}),$$

where $\mathbf{b}_i, \mathbf{b}_j : \mathbb{R} \times \mathbb{R}^n \rightarrow \mathbb{R}^n$ are continuously differentiable vector fields. The LBS in (4) represents a gradient-like system [38, 48, 49] that averages the dynamics of the ESC

system in (3) [39]. Now we turn our attention to a special case (subclass) of control-affine ESC systems in (3) [48], which includes various control-affine ESC designs commonly found in the literature (e.g., [13, 38, 47, 49, 52–54]), including unicycle-based ESC designs and the very simple ESC law in (1). Said subclass in the single-dimension case (i.e., $n = 1$) can be expressed as:

$$\dot{x} = b_1(f(x))u_1 + b_2(f(x))u_2, \quad (5)$$

where $f(x)$ represents the objective function, and the terms b_1 and b_2 are the vector fields associated with the perturbation/excitation signals u_1 and u_2 , respectively. The generalized structure of ESC systems in the form of (5) is shown in the unshaded portions of Figure 4 [49], where the excitation signals are defined as $u_1 = a\sqrt{\omega}\hat{u}_1(\omega t)$ and $u_2 = a\sqrt{\omega}\hat{u}_2(\omega t)$. Here, $a \in \mathbb{R}$ represents the amplitude of the excitation signal. Moreover, the corresponding LBS to the ESC system in (5) is given by [48]:

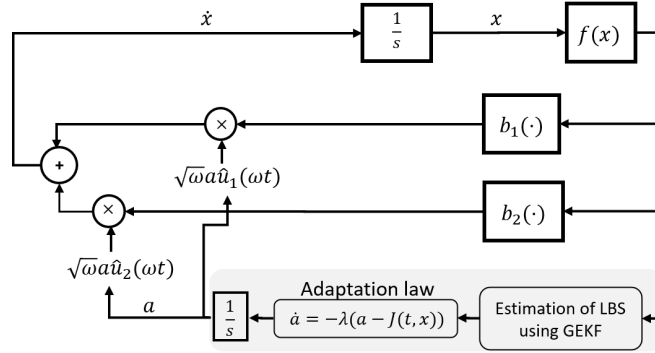


Figure 4: The proposed ESC design in [49].

$$\dot{z} = -\nu_{2,1}\nabla f(z)b_0(f(z)), \quad \text{where} \quad b_0(z) = b_2(z)\frac{db_1(z)}{dz} - b_1(z)\frac{db_2(z)}{dz}, \quad z \in \mathbb{R}. \quad (6)$$

For multi-variable ESC (higher dimensions), the structure in (5) becomes:

$$\dot{\mathbf{x}} = \sum_{i=1}^n (b_{1i}(f(\mathbf{x}))u_{1i} + b_{2i}(f(\mathbf{x}))u_{2i}) e_i, \quad (7)$$

where $f : \mathbb{R}^n \rightarrow \mathbb{R}$, and e_i is the i^{th} unit vector in \mathbb{R}^n . Similarly, the corresponding LBS to the ESC system in (7) is:

$$\dot{\mathbf{z}} = -\sum_{i=1}^n \nu_{2i,1i} \frac{\partial f(\mathbf{z})}{\partial z_i} b_{0i}(f(\mathbf{z})) e_i. \quad (8)$$

We assume that the following assumptions from [49] hold:

- A1. $b_{ji}, b_{ji} \in C^2 : \mathbb{R} \rightarrow \mathbb{R}$, and for a compact set $\mathcal{C} \subseteq \mathbb{R}$, there exist $A_1, \dots, A_3 \in [0, \infty)$ such that $|b_j(x)| \leq A_1$, $|\frac{\partial b_j(x)}{\partial x}| \leq A_2$, $|\frac{\partial [b_j, b_k](x)}{\partial x}| \leq A_3$ for all $x \in \mathcal{C}$, $i = 1, 2$; $j = 1, 2$; $k = 1, 2$.

- A2. $\hat{u}_{1i}, \hat{u}_{2i} : \mathbb{R} \times \mathbb{R} \rightarrow \mathbb{R}, i = 1, 2$, are measurable functions. Moreover, there exist constants $M_i \in (0, \infty)$ that $\sup_{\omega t \in \mathbb{R}} |\hat{u}_i(\omega t)| \leq M_i$, and $\hat{u}_i(\cdot)$ is T-periodic, i.e. $\hat{u}_i(\omega t + T) = \hat{u}_i(\omega t)$, and has zero average, i.e. $\int_0^T \hat{u}_i(\tau) d\tau = 0$, with $T \in (0, \infty)$ for all $\omega t \in \mathbb{R}$.
- A3. There exists an $x^* \in \mathcal{C}$ such that $\nabla f(x^*) = 0, \nabla f(x) \neq 0$ for all $x \in \mathcal{C} \setminus \{x^*\}$; $f(x^*) = f^* \in \mathbb{R}$ is an isolated extremum value.

Assumptions A1-A3 are typical in ESC literature – see for example [38, 39, 49, 50]. A1-A2 ensure well-posedness, boundedness, zero-mean average, and measurability of the excitation signals. A3 ensures the objective function f has an isolated local extremum (maximum/minimum) f^* at \mathbf{x}^* . Typically, the stability analysis and the design process of a control-affine ESC system is done via the approximating/corresponding LBS [39]. Now we recall the following stability results [38, 39, 48] that relate the stability of the LBS in (6) with the ESC system in (5) (or more generally, the stability of the LBS in (8) with the ESC system in (7)).

Theorem 1. *Let assumptions A1-A3 be satisfied and suppose that a compact set \mathcal{C} is locally (uniformly) asymptotically stable for (8). Then \mathcal{C} is locally practically (uniformly) asymptotically stable for (7).*

Readers who are not familiar with the concept of practical stability can refer to [38, 39] for formal definitions, but can think about practical stability as, roughly speaking, a form of Lyapunov stability (trajectories are bounded and stay close to the equilibrium). That is, if the LBS (which is an autonomous averaged system) converges asymptotically to the extremum point (maximum/minimum of the objective function), then the ESC system will be bounded within a certain radius from said extremum point (e.g., oscillates around it).

2.3. Geometric-based Extended Kalman Filtering

Geometric-based Extended Kalman Filtering (GEKF) [50] is a filtering technique that was developed very recently to estimate unknown parameters/variables in control-affine systems, particularly, control-affine ESC systems of the form (7). GEKF has been proven very effective/useful in improving the performance of control-affine ESC systems, enabling new class of ESC systems with attenuating oscillations instead of persisting oscillations (i.e., achieving asymptotic stability instead of practical stability) – see Figure 4 and out theoretical results in [49]. Below, we briefly provide the idea and equations of design of GEKF and its coupling with control-affine ESC systems.

The LBS in (8) can be determined using measurements of the objective function $f(\mathbf{x})$ and predefined structural parameters. Therefore, the estimation of the LBS, which captures the qualitative behavior of the ESC, including how close or far it is from reaching the extremum, inherently depends on the gradient of the objective function. That is, if one is able to estimate the gradient of $f(\mathbf{x})$ (i.e., $\nabla f(\mathbf{x})$), then one is automatically able to estimate the LBS in (8). To address this, the concept of the

estimated LBS, denoted as $\hat{\mathbf{z}}$ is addressed, which is defined as follows [50]:

$$\dot{\hat{\mathbf{z}}} = - \sum_{i=1}^n \left(\nu_{2i,1i} \frac{\partial f(\mathbf{z})}{\partial z_i} b_{0i}(f(\mathbf{z})) + \eta_i(t) \right) e_i = \mathbf{J}(t, \mathbf{z}). \quad (9)$$

The form of the estimated LBS in (9) closely resembles the LBS described in (8), with the key difference being the inclusion of an error term $\eta_i(t)$, which accounts for measurements noise during the estimation process. To ensure that the error term $\eta_i(t)$ is measurable, uniformly bounded, and diminishes over time, the following assumption is imposed [49, 50]:

A4. $\eta_i(t) : \mathbb{R} \rightarrow \mathbb{R}$, $i = 1, \dots, n$ is a measurable function, and there exist constants $\theta_0, \epsilon_0 \in (0, \infty)$ such that $|\eta_i(t_2) - \eta_i(t_1)| \leq \theta_0 |t_2 - t_1| \forall t_1, t_2 \in \mathbb{R}$, $\sup_{t \in \mathbb{R}} |\eta_i(t)| \leq \epsilon_0$, and $\lim_{t \rightarrow \infty} \eta_i(t) = 0$.

Assuming one has access to the estimated LBS (9) with estimation abiding by the assumption A4, a class of control-affine ESC has been proposed successfully in [49] that couples the control-affine ESC system in (7) with an adaptation law for the amplitude of the excitation signal that relies on the estimated LBS as also shown in Figure 4 including the shaded area. Said ESC class is expressed as follows [49]:

$$\dot{\mathbf{x}} = \sum_{i=1}^n (b_{1i}(f(\mathbf{x})) \sqrt{\omega} a_i(t) \hat{u}_{1i} + b_{2i}(f(\mathbf{x})) \sqrt{\omega} a_i(t) \hat{u}_{2i}) e_i, \quad (10)$$

$$\dot{\mathbf{a}} = \sum_{i=1}^n (-\lambda_i (a_i(t) - J_i(t, \mathbf{x}))) e_i, \quad (11)$$

where $J_i(t, \mathbf{x})$ represents the right-hand side of the estimated LBS (see (9)), $\mathbf{x} \in \mathcal{C} \subset \mathbb{R}^n$ and $a_i \in \mathbb{R}$ represents the amplitude of the input signal, $\lambda_i > 0 \in \mathbb{R}$ is a tuning parameter, and $u_i = a_i \hat{u}_i$.

The ESC class in (10)-(11) provides designs guaranteed to attenuate in oscillations, resolving the known persisting oscillation problem in ESC literature. The applicability/functionality of the ESC class in (10)-(11) relies on the estimations of the gradient of the unknown objective function $f(\mathbf{x})$ (i.e., $\nabla f(\mathbf{x})$), which in turn provides $J_i(t, \mathbf{x})$. Said estimations is guaranteed to have high precision with an error that vanishes as $t \rightarrow \infty$ as in A4 via GEKF [49]. As in [49, 50], GEKF operates in real-time as a discrete-continuous extended Kalman filter. Its implementation relies on two essential components: a measurement equation, which serves as the discrete part of the filter by linking the gradient of the objective function $\nabla f(\mathbf{x})$ to the available measurements of $f(\mathbf{x})$, and a propagation model, which acts as the continuous part and governs the filter's behavior between successive discrete measurement updates. The GEKF is built upon the Chen-Fliess series expansion (see the Appendix for more details, and set $y = f(x)$ in (1)). By truncating the series after first-order terms, the following relation is obtained:

$$f(\mathbf{x})|_{t_2} = f(\mathbf{x})|_{t_1} + \mathbf{b}_1 \cdot \nabla f(\mathbf{x})|_{t_1} U_1 + \mathbf{b}_2 \cdot \nabla f(\mathbf{x})|_{t_1} U_2 + O((\Delta t)^2), \quad (12)$$

where $U_1 = \int_{t_1}^{t_2} u_1 d\tau$ and $U_2 = \int_{t_1}^{t_2} u_2 d\tau$, with $t_2 = t_1 + \Delta t$. The time step Δt is chosen to be small relative to the periodic duration of the input signal, such that $\Delta t = K/\omega$, where K is a constant. Higher-order terms, represented by $O(1/\omega^2)$, become negligible at sufficiently high frequencies. This truncated relationship has been utilized as the measurement update equation in the GEKF for estimating the LBS. The GEKF state variables for gradient estimation is [50]:

$$\bar{\mathbf{X}} = \begin{bmatrix} \bar{\mathbf{x}}_1 \\ \bar{\mathbf{x}}_2 \\ \bar{x}_3 \end{bmatrix} = \begin{bmatrix} -\sum_{i=1}^n \nu_{2i,1i} \frac{\partial f(\mathbf{x})}{\partial x_i} b_{0i}(f(\mathbf{x})) e_i \\ \dot{\bar{\mathbf{x}}}_1 \\ f(\mathbf{x})|_{t_1} \end{bmatrix}, \quad (13)$$

where $\bar{\mathbf{x}}_1$ corresponds to the right-hand side of the LBS in (8), $\bar{\mathbf{x}}_2$ represents its constant derivative, and \bar{x}_3 captures the constant value of the objective function evaluated at t_1 . The system's behavior between measurement updates is described by the following state propagation model:

$$\dot{\bar{\mathbf{X}}} = \begin{bmatrix} \bar{\mathbf{x}}_2 \\ 0 \\ 0 \end{bmatrix} + \mathbf{\Omega}, \quad (14)$$

where $\mathbf{\Omega}$ denotes the process noise vector, assumed to follow a Gaussian distribution with zero mean and covariance matrix \mathbf{Q} . Additionally, the process noise is considered uncorrelated with the measurement noise. For a detailed explanation of the GEKF, including its concept, steps, applications, and solved examples, readers are encouraged to refer to [16, 50]. More importantly, GEKF has been tested successfully in robotic experiments, and in source-seeking by improved single-integrator application – see [12].

3. Proposed Unicycle-Based Extremum Seeking Controller Design and Algorithm for Model-Free, Real-Time Source-Seeking

In this section, we provide our proposed unicycle-based ESC design, which can be considered as a bio-inspired approach that is particularly useful for differential wheeled robots. We provide the block diagram of the design, its state space representation, and an implementation algorithm for real-world source-seeking robotic applications.

3.1. Structure and Rationale of the Proposed Unicycle-Based ESC Design

Let us now construct the rationale of our proposed design in three steps. Firstly, we start by reconsidering the unicycle dynamics described in (2) but with only a single control input that is the linear velocity v (i.e., $u = v$) and a fixed angular velocity Ω . Secondly, we propose using the structure of the very simple ESC law in (1) to determine the update of the linear velocity v . We also apply a high-pass filter (HPF) to the measurement of

the objective function $f(x, y)$ to improve the transient behavior and the accuracy of sensor measurements. That is, $u = v = (f(x, y) - eh)u_1 + u_2$, where u_1 and u_2 are the ESC perturbation/excitation signals (usually are taken as sinusoidal signals, but other forms are allowed as long as they satisfy assumption A2), e is the resulting state from using the HPF with constant h that is greater than or equals to zero (note that if $h = 0$, we get $u = v$ exactly as the law in (1)). Thirdly, we turn the unicycle dynamics with the aforementioned considerations to be effectively a member of our recent ESC class proposed in [49] to guarantee attenuating oscillations and better performance due to the use of GEKF that enables better handling of sensor noise and complete stopping at the source if it is a fixed one. That is, our unicycle-based ESC follows the state space representation in (10)-(11), incorporating an adaptation mechanism that reduces the amplitude a of the perturbation/excitation signals u_1 and u_2 . Hence, the linear velocity v will automatically have lesser perturbations as it gets closer to the terminal/desired source the robot is seeking (i.e., v perturbs as needed and vanishes at the source the robot is seeking). However, our proposed design is proven to be capable of tracking moving source as well; this will be shown in Section 4.3. The proposed unicycle-based ESC design operates in a planar mode (x and y coordinates) with $u_1 = \sin(\omega t)$ and $u_2 = \cos(\omega t)$, where ω is the perturbation/excitation frequency. The proposed design has the following state space representation:

$$\begin{aligned}
 \dot{x} &= ((f(x, y) - eh) c\sqrt{\omega} \sin(\omega t) + a\sqrt{\omega} \cos(\omega t)) \cos \Omega t, \\
 \dot{y} &= ((f(x, y) - eh) c\sqrt{\omega} \sin(\omega t) + a\sqrt{\omega} \cos(\omega t)) \sin \Omega t, \\
 \dot{e} &= -he + f(x, y), \\
 \dot{a} &= -\lambda(a - J(x, y)),
 \end{aligned} \tag{15}$$

where c and λ are tuning constants. Furthermore, the proposed unicycle-based ESC design is provided in Figure 5. Additionally, the LBS corresponding to the first three

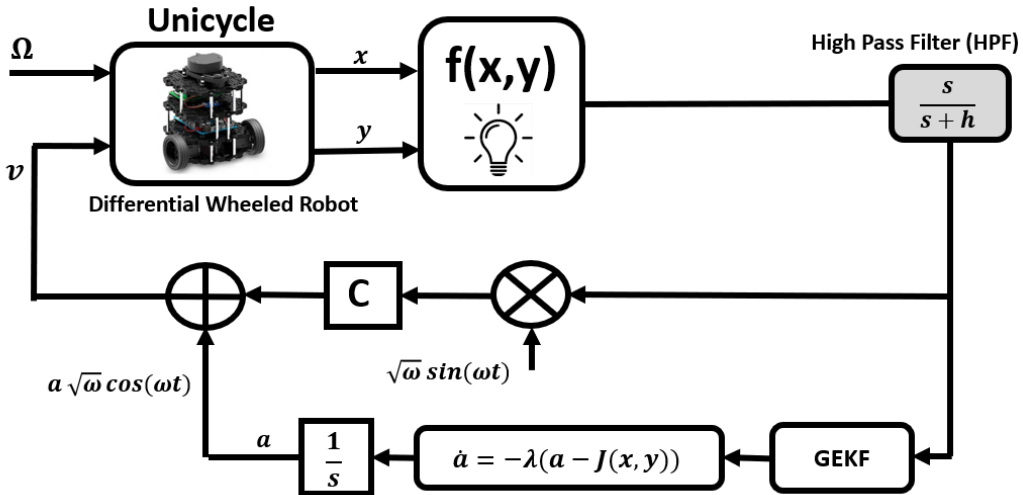


Figure 5: The proposed unicycle-based ESC design

equations in (15) that will be used for the GEKF implementation (to determine $J(x, y)$), is based on (8) and is obtained as follows:

$$\begin{bmatrix} \dot{\bar{x}} \\ \dot{\bar{y}} \\ \dot{\bar{e}} \end{bmatrix} = \frac{1}{2} \begin{bmatrix} ca \nabla_x f(x, y) \cos^2(\Omega t) \\ ca \nabla_y f(x, y) \sin^2(\Omega t) \\ 2(-\bar{e}h + f(x, y)) \end{bmatrix}. \quad (16)$$

3.2. GEKF Design Details: Calculations and Implementation Algorithm

For successful implementation of the proposed design (Figure 5), we need to derive the GEKF for the proposed design. Let us recall the general formulation and steps in Section 2.3 and customize them for the proposed design. Based on (13), the proposed GEKF will have five states. The first two states of the proposed GEKF will be the first two entries of the right-hand side of the LBS in (15). Then, the third and fourth states of the proposed GEKF will be the derivatives of the first and second states themselves of the proposed GEKF, respectively. The fifth and last state will be the the third entry of the right-hand side of the LBS in (15). As a result, the proposed GEKF states are defined as follows:

$$\bar{\mathbf{X}} = \begin{bmatrix} \bar{x}_1 \\ \bar{x}_2 \\ \bar{x}_3 \\ \bar{x}_4 \\ \bar{x}_5 \end{bmatrix} = \begin{bmatrix} \frac{ca}{2} \nabla_x f(x, y) \cos^2(\Omega t)|_{t_1} \\ \frac{ca}{2} \nabla_y f(x, y) \sin^2(\Omega t)|_{t_1} \\ \dot{\bar{x}}_1 \\ \dot{\bar{x}}_2 \\ (f(x, y) - eh)|_{t_1} \end{bmatrix}_{5 \times 1}. \quad (17)$$

Using a constant velocity propagation model as in (14), we get:

$$\dot{\bar{\mathbf{X}}} = \begin{bmatrix} \bar{\mathbf{x}}_3 \\ \bar{\mathbf{x}}_4 \\ 0 \\ 0 \\ 0 \end{bmatrix}_{5 \times 1} + \mathbf{\Omega}, \quad (18)$$

where $\mathbf{\Omega}$ denotes the process noise vector modeled as a random variable, \mathbf{Q} represents the covariance matrix associated with the process noise (system noise), and the Jacobian matrix \mathbf{A} , corresponding to the state dynamics, is computed as:

$$\mathbf{A} = \begin{bmatrix} 0 & 0 & 1 & 0 & 0 \\ 0 & 0 & 0 & 1 & 0 \\ 0 & 0 & 0 & 0 & 0 \\ 0 & 0 & 0 & 0 & 0 \\ 0 & 0 & 0 & 0 & 0 \end{bmatrix}_{5 \times 5}. \quad (19)$$

For the measurement updates, the Chen-Fliess series expansion is utilized as explained in Section 2.3 and as detailed in [49, 50]. In short, we utilize (12) but with $f(x, y)$

replaced with $(f(x, y) - eh)$. Using the Chen-Fliess series expansion and truncating the series after the first-order terms, we obtain:

$$\begin{aligned}
(f(x, y) - eh)|_{t_2} &= (f(x, y) - eh)|_{t_1} + (\nabla f(x, y) \cdot \mathbf{b}_1)|_{t_1} K \cos(\omega t) \\
&\quad + (\nabla f(x, y) \cdot \mathbf{b}_2)|_{t_1} K \sin(\omega t) + \nu(t), \\
\text{where } \mathbf{b}_1 &= \begin{bmatrix} c(f(x, y) - eh) \cos(\Omega t) \\ c(f(x, y) - eh) \sin(\Omega t) \\ 0 \end{bmatrix}, \\
\mathbf{b}_2 &= \begin{bmatrix} a \cos(\Omega t) \\ a \sin(\Omega t) \\ 0 \end{bmatrix},
\end{aligned} \tag{20}$$

and $t_2 = t_1 + \Delta t$. Based on the approach in [49, 50], K is defined as $K = \frac{2}{\sqrt{\omega}} \sin\left(\frac{\omega \Delta t}{2}\right)$, where Δt denotes a small time step between measurements. It is critical to ensure that Δt is significantly smaller than the period of the input signal. The residual terms are assumed to follow a Gaussian distribution representing measurement noise, denoted as $\nu(t) \sim N(0, R)$, where R is the covariance matrix associated with the noise. The measurement update equation can then be rewritten in terms of the GEKF states as:

$$\begin{aligned}
(f(x, y) - eh)|_{t_2} &= (f(x, y) - eh)|_{t_1} + \left(\nabla_x f(x, y)(f(x, y) - eh)c \cos(\Omega t) \right. \\
&\quad \left. + \nabla_y f(x, y)(f(x, y) - eh)c \sin(\Omega t) \right) K \cos(\omega t) \\
&\quad + \left(\nabla_x f(x, y)a \cos(\Omega t) + \nabla_y f(x, y)a \sin(\Omega t) \right) K \sin(\omega t) + \nu(t), \\
&= \bar{x}_5 + \frac{2K}{a \cos(\Omega t)} \bar{x}_1 \bar{x}_5 \cos(\omega t) + \frac{2K}{a \sin(\Omega t)} \bar{x}_2 \bar{x}_5 \cos(\omega t) \\
&\quad + \frac{2K}{c \cos(\Omega t)} \bar{x}_1 \sin(\omega t) + \frac{2K}{c \sin(\Omega t)} \bar{x}_2 \sin(\omega t) + \nu(t).
\end{aligned}$$

where $t = (t_1 + t_2)/2$. The Jacobian matrix associated with the measurement update equation is:

$$\mathbf{C} = \begin{bmatrix} \frac{2K}{a \cos(\Omega t)} \bar{x}_5 \cos(\omega t) + \frac{2K}{c \cos(\Omega t)} \sin(\omega t) \\ \frac{2K}{a \sin(\Omega t)} \bar{x}_5 \cos(\omega t) + \frac{2K}{c \sin(\Omega t)} \sin(\omega t) \\ 0 \\ 0 \\ 1 + \frac{2K}{a \cos(\Omega t)} \bar{x}_1 \cos(\omega t) + \frac{2K}{a \sin(\Omega t)} \bar{x}_2 \cos(\omega t) \end{bmatrix}^T. \tag{21}$$

Now we are in a position to provide Algorithm 1, which is an implementation algorithm for the proposed unicycle-based ESC design operating with GEKF as in Figure 5. The GEKF operates by propagating the state estimate and covariance through the prediction step, followed by measurement updates whenever new sensor data is available. Since the operation of GEKF is necessary for the attenuation of oscillations (incurring adaptive

perturbation/excitation) via reducing the amplitude a (see Figure 5), then we can effectively introduce a stopping condition when a is smaller than a certain very small threshold ϵ (e.g., $\epsilon = 0.01$) as this indicates that the robot has practically reached the source. Said stopping condition will be applied via the only control input v (the linear velocity). That is, if $a \leq \epsilon$, then the input is $v = 0$, effectively halting its motion. Otherwise, the GEKF continues to estimate the system states.

Algorithm 1 Unicycle-based Source Seeking Algorithm (Using GEKF)

Initialization:

- Set the initial state estimate $\bar{\mathbf{X}}$ in (17).
- Select the output sample time Δt , ensuring that it is lower than the sensor sampling rate.
- Select N as the number of discrete subintervals within Δt for improving the accuracy of the prediction step.
- Set the threshold value ϵ that determines when the algorithm stops (e.g., ϵ can be a small positive value like 0.01).

Simulation Begins: (the system (15) is active)

- Track the amplitude of the oscillatory input signal a (the last variable in (15)) to assess whether the system dynamics need to continue in activation or stop.

if $a > \epsilon$ then

Start Estimating State $\bar{\mathbf{X}}$:

for $i = 1$ to N do (Prediction Step)

- $\bar{\mathbf{X}} = \bar{\mathbf{X}} + (\Delta t/N)\dot{\bar{\mathbf{X}}}$
- $\mathbf{P} = \mathbf{P} + \frac{\Delta t}{N}(\mathbf{A}\mathbf{P} + \mathbf{P}\mathbf{A}^T + \mathbf{Q})$

• End for

Return: $\bar{\mathbf{X}}$ and \mathbf{P} .

Measurement Update:

- When a new measurement is received from the sensor, perform the following:
- $\mathbf{C} = \frac{\partial h}{\partial \bar{\mathbf{X}}}(\bar{\mathbf{X}})$ (Jacobian from (21)).
- $\mathbf{L} = \mathbf{P}\mathbf{C}^T(\mathbf{R} + \mathbf{C}\mathbf{P}\mathbf{C}^T)^{-1}$
- $\mathbf{P} = (\mathbf{I} - \mathbf{L}\mathbf{C})\mathbf{P}$ (Update the covariance matrix).
- $\bar{\mathbf{X}} = \bar{\mathbf{X}} + \mathbf{L}(\mathbf{y} - \mathbf{C}\bar{\mathbf{X}})$ (Update the state estimate).

else ($a \leq \epsilon$)

Stop the System:

- Set the velocity $v = 0$.

• End if

3.3. Discussion and Comments on the Proposed Design and its Advantages Compared to the Literature

It is important to observe that our unicycle-based ESC design (Figure 5) does not require any integrators for the states. That is, differential wheeled robots (e.g., Turtlebot3 [45]) need its input command to be the velocities (i.e., v and Ω). Hence, as noted in Figure 5, the update of v is the only external design element needed for operability; note that in our design Ω is fixed, effectively making the source-seeking problem a single-input (i.e., v), single-output (i.e., $f(x, y)$), model-free and real-time design. This is quite advantageous for practical applications as it reduces the complexities of the control architecture and all relevant complications. However, it is important to mention that the structure of the ESC law for the input v is a very important factor in performance consideration, because in real-world implementation, the ESC law for v will be naturally processed and discretized. That is, the update of the input v due to the ESC law will not be a continuous update, but will be samples of updates (input) data. As a result, the purity and simplicity of the ESC law for v should be leveraged whenever possible as will be discussed in the following paragraph.

In our proposed design (Figure 5), we used the very simple ESC law in (1) for v . For this law to be in effect, one only needs to multiply the measurements (samples received from the sensor) of $f(x, y)$ after passing through a high-pass filter with a sinusoidal signal, then adds the resultant quantity to another sinusoidal signal. Thus, in reality, in order to use the simple ESC law (1) in real-world applications, one needs only careful choice of the sinusoidal signals to make sure they discretize in a way that keeps the excitation of the ESC intact. In other words, one does not have to worry when using the ESC law in (1) about discretization that involves the already sampled $f(x, y)$ due to the use of sensors, but directly use the sampled data themselves without extra processing while having full control in choosing the discretization rate and frequency of the excitation sinusoidal signals that align well with the sensor measurements rate. It is worth noting that discretization of sinusoidal signals have been a major topic in the digital communication field and most platforms and processors are well accustomed to it, which suggests further the practicality of using the ESC law in (1), especially in mobile robotic applications.

The natural question that arises: why the simple ESC law in (1) did not find successes to be considered in effective real-world robotic applications (e.g., source-seeking) even though it has been around for, at least, over a decade [38]? The answer simply is that, for about a decade, the ESC law in (1) has been considered to be ineffective. It has been shown that it suffers from persistent oscillations [48]. Also, it has been shown to perform poorly in robotic experimental works, including with a differential wheeled robot [13]. It was not until our recent work [49] that we showed the ESC law in (1) can, in fact, work effectively with attenuating oscillations using GEKF. This has been validated experimentally for single-integrator designs (not unicycle-based designs) in our recent work [12]. In said work, the use of GEKF not only enabled effective

use of the ESC law in (1), it has shown significant ability to improve the convergence rate and improve the handling of noise. Thus, it is only natural to do the work of this paper and provide a unicycle-based ESC design using the law in (1) for all of its technical advantages we discussed in earlier paragraphs, accompanied with GEKF for attenuation of oscillations and other performance improvements such as those observed in the single-integrator case [12]: better handling of noise and improved convergence rate. Even though our recently proposed ESC class [49], which we build upon on this work, can admit other control laws such as those used in [13, 48], we preferred to only consider the ESC law in (1) as these other laws involve compositions of maps that is applied to the sampled measurements of $f(x, y)$. As a result, these can be challenging structures at most, and require at least more careful study/considerations for how discretizations and processing of data can be (and should be) performed given the multi-layer processing of eminently – due to the use of sensors – noisy sampled measurements of $f(x, y)$.

4. Simulation and Differential Wheeled Robotic Experimental Results

In this section, we provide simulation and experimental results for our proposed unicycle-based ESC design, as presented in Section 3, to ensure validation and verification of the proposed design, and to demonstrate its applicability/relevance to robotic applications, such as fixed and moving source-seeking. Furthermore, the experimental results provided in this section validate the recent theoretical results in [49] and their applicability in robotics. All simulations are performed using MATLAB[®]. For the experimental validation presented in this section, we used a differential wheeled robot, namely Turtlebot3 (TB3) robot [45]. TB3 is a compact, cost-effective, differential-drive mobile robot platform based on ROS (Robot Operating System). Developed by ROBOTICS, it is tailored for research and educational purposes. The TB3 comes in two variants: Burger and Waffle. In this study, we utilized the Burger variant, which features a wheelbase of 160 mm and a wheel radius of 33 mm. The robot depicted in Figure 1 and Figure 5 is, in fact, an instance of the TB3. Figure 6 provides an overview of the experimental configuration used in our laboratory. The setup comprises three primary components. The first component (labeled #1) is the TB3 robot itself. The second component (labeled #2) is the light source, which acts as the extremum or target source for the experiments and can be replaced by any objective in the context of ESC systems. Finally, the third component (labeled #3) is the motion capture system, which is used to track and visualize the planar trajectory of the TB3 during the experiments.

4.1. Simulation and Experimental Results for a Known Objective Function

This subsection presents the details, results, and observations of the first phase of our study. In this phase, we implement our proposed unicycle-based ESC design using a known mathematical expression for the objective function $f(x, y)$, which is utilized solely for obtaining measurements. The effectiveness of the proposed design is first

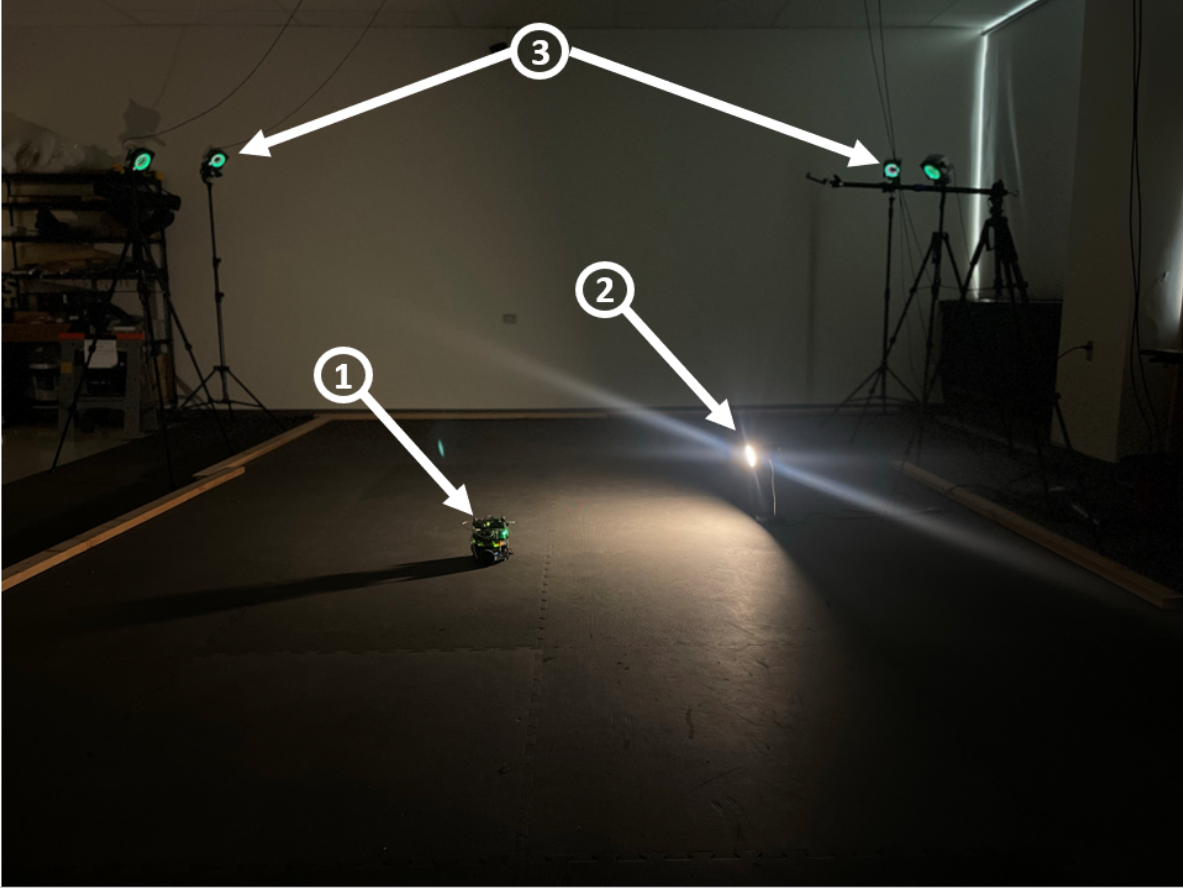


Figure 6: Modeling, Dynamics, and Control Lab (MDCL) [55]. (#1). TB3 inside the testing area, (#2). A light source, and (#3). Motion capturing system (MCS).

evaluated through simulations conducted using MATLAB and Simulink[®]. Below, we provide detailed descriptions of the conducted simulations.

The initial conditions for the states (x, y) are set to $(2, 2)$. For the GEKF, the initial value of the covariance matrix P is chosen as $[4, 4, 4, 4, 4]^T$, with a sample rate of $\Delta t = 0.01$, $\mathbf{Q} = 0.0005\mathbf{I}$ (where \mathbf{I} is the identity matrix), $R = 0.00999$, and $N = 10$. For the ESC parameters, we use $\omega = 120$, $c = 0.3$, and $\Omega = 3 \text{ rad/s}$. The adaptation law starts with initial conditions $a(0) = 1$ and $\lambda = 0.0105$. For simulations without GEKF and adaptation law, $a = \text{constant} = 1$. The HPF constant is taken as $h = 1$. The objective function employed for obtaining measurements is $f(x, y) = 10 - \frac{1}{2}(x - 1)^2 - \frac{3}{2}(y - 1)^2$, which has a clear extremum (maximum) at $f^* = 10$ when $(x, y) = (1, 1)$. The simulation results are presented in Figure 7, illustrating the x - and y -states as well as the planar trajectory. From Figure 7, it is clear that our proposed design, incorporating the GEKF, effectively attenuates oscillations and asymptotically converges to the maximum points for x and y . As expected, the planar trajectory (x vs. y) demonstrates convergence with reduced oscillations. These simulation results validate that our proposed design that with GEKF, outperforms the literature design (without GEKF) by achieving faster convergence and significantly

attenuating oscillations, thereby demonstrating better performance.

Moving forward, we extended our study to real-world, real-time experiments using the same known objective function as in the simulations to obtain measurements. These experiments were conducted to validate the performance of our proposed unicycle-based ESC design with GEKF (see Algorithm 1). The results were compared against a baseline design from the literature (without GEKF, i.e., only the first three equations in (15) are in effect, like the unicycle ESC design in [38]). For the experimental setup, the following parameters were used: the initial state values (x, y) were set to $(2, 2)$; the covariance matrix P was initialized as $[4, 4, 4, 4, 4]^T$; the sample rate was $\Delta t = 0.1$; and $\mathbf{Q} = 0.0005\mathbf{I}$, $R = 0.5$, and $N = 20$ were chosen. For the ESC parameters, $\omega = 50$, $c = 5$, and $\Omega = 1.75$ rad/s were used. The adaptation law was initialized with $a(0) = 3.53$ and $\lambda = 0.01$. For HPF constant, $h = 1$ was applied.

The experimental results are presented in Figure 8. The performance of our proposed design is noteworthy, as this is the first experimental demonstration of a unicycle-based ESC system incorporating GEKF. As seen in the figure, the x - and y -states successfully converged asymptotically to the desired maximum point $(1, 1)$ with significantly attenuated oscillations. It is important to highlight that, by using the GEKF and the stopping condition in the Algorithm 1, the robot arrived successfully at the source (maximum point) and then stopped, taking approximately 350 seconds – see the x - and y -coordinate plots (first two subplots in Figure 8). In comparison, the baseline design (without GEKF as explained earlier) took a significantly longer time (around 2000 seconds) to reach about the target location with persistent oscillations.

Two important observations are worth noting. First, the slight variations observed in the x - and y -plots after 350 seconds, when the robot had already stopped at the target point, are attributed to noise from the Motion Capturing System (MCS) used for plotting the trajectory. Second, due to the physical constraints of the TB3 robot on linear velocity (maximum 0.22 m/s) and angular velocity (maximum 2.8 rad/s), the TB3 robot is relatively slow. Hence, performance comparisons between our proposed design and the baseline design in the literature should be understood and observed in a relative sense. Indeed, faster and more capable robots can provide higher absolute speeds as needed.

Finally, the planar trajectory plot (see third subplots in Figure 8) further highlights that the proposed design enabled the TB3 to reach the maximum position following a shorter and more efficient path compared to the baseline design, demonstrating an improved convergence rate. Moreover, for a better qualitative evaluation, and since we have access to the mathematical expression of the objective function, one can compute the LBS for the planner trajectory. The reader is directed to the Appendix, particularly equation (.7), for derivation of the LBS. It is evident from the third subplots in Figure 8 that the proposed design allowed the robot to follow the LBS system trajectory (blue) more closely and accurately, with significantly reduced oscillations and faster convergence to the maximum. This validates the effectiveness of our GEKF algorithm in providing a more accurate estimation of the LBS system and achieving

superior performance. For enhanced visualization, we have provided a YouTube video showing the experimental results for our proposed design, accessible via [56] and for the baseline design accessible via [57]. It is important to emphasize that the attenuation of oscillations and asymptotic convergence observed in these experiments strongly supports the theoretical predictions outlined in [49]. Interestingly, the improved convergence rate, a previously unexplored aspect, indicates that the GEKF provides additional advantages for control-affine ESC systems. This finding suggests that further investigations of the broader implications of using GEKF in such systems could be highly beneficial.

4.2. Experimentation of the Proposed Design for Model-free, Real-time Source-Seeking of Fixed Light Source

To further validate and verify the effectiveness of our proposed unicycle-based ESC design, we conducted an additional phase of real-world, real-time experiments, where we implemented Algorithm 1 on the TB3 robot. In this phase, the light intensity distribution was used as the unknown objective function, with measurements obtained via a light sensor. The extremum corresponds to the position of the maximum light intensity, representing the source position (a source-seeking problem). Importantly, this experiment was entirely model-free, as no mathematical expression was used to describe the TB3 robot, the sensor, or the light distribution. We implemented the proposed design with GEKF and compared its performance against a baseline design from the literature (without GEKF as described in Section 4.1).

For these experiments, the initial state values (x, y) were set to $(1.3, 0.85)$, the covariance matrix P was initialized as $[4, 4, 4, 4, 4]^T$, and the sample rate was $\Delta t = 0.1$. The noise covariance matrices were $\mathbf{Q} = 0.005\mathbf{I}$ and $R = 0.2$, while the number of subintervals was $N = 20$. The ESC parameters were chosen as $\omega = 100$, $c = 1$, and $\Omega = 1$ rad/s. The adaptation law was initialized with $a(0) = 0.55$, and the tuning parameters were $\lambda = 0.02$. The HPF constant was taken as $h = 6$. For the baseline design (without GEKF), the parameter $a = \text{constant} = 1$ was used.

The experimental results are presented in Figure 9. These experiments demonstrated that the proposed design successfully steered autonomously the TB3 robot to the light source, achieving attenuated oscillations and faster convergence compared to the baseline design without GEKF. This is clearly shown in the x - and y -coordinate subplots of Figure 9, where the robot using the proposed design reached the target light source and stopped upon arrival (in less than 24 seconds), as indicated by the stabilized x - and y -coordinates. On the other hand, the baseline literature design did not perform that well; it took the robot much longer time (compared to the proposed design) to reach about the light source, but with very noisy and persistent oscillations.

Finally, the planar trajectory subplots in Figure 9 further highlight the effectiveness of the proposed design compared to the baseline literature design. The planner trajectory generated by the robot using the proposed design (Algorithm 1) is shorter and less challenging (i.e., more efficient) as apposed to the planner trajectory generated by the

baseline literature design. For enhanced visualization, we have created a YouTube video showcasing the experimental results for our proposed design, accessible at [58] and for the baseline design accessible via [59].

4.3. The Ability of Our Proposed Design to Track a Moving Light Source

To further test the capabilities of the proposed design, we explored its performance in a dynamic scenario where the light source position changes over time, which represents a relatively slow time-varying extremum (slowly moving/drifting source). Our adaptation law for a (see Figure 5 and Eq. (15)) updates the amplitude of the excitation/perturbation signal based on – roughly speaking – the system’s distance from the extremum (source). Closer to the extremum (source), smaller perturbations are required to extract gradient information, while further from the extremum, larger perturbations are necessary. Hence, as can be seen in Algorithm 1, the proposed design attenuates oscillations resulting from excitation/perturbation signals as the robot gets closer to the source. Our experiments until now (Sections 4.1 and 4.2) successfully demonstrated the ability of the proposed design to dynamically adjust oscillations by attenuation, allowing the TB3 robot to track the source effectively and stop at it. However, in order to test if the proposed design, via its adaptation law, can also increase perturbations (oscillations) if it needs more excitation to track a source with a moving/changing position, we needed to conduct another experiment. In this experiment, we fixed the light source at an initial position, then started the source-seeking procedure (i.e., activated Algorithm 1). Once the TB3 robot reached the light source at the initial position with attenuated oscillations, we then moved the light source position to another place to test if the proposed design, via its adaptation law for a , is able to increase the excitation (oscillation) that is now needed to track the new light source position. In this experiment, we moved the light source three times and the proposed design was successful, and operated effectively, tracking the moving light source. The results of this experiment is presented in Figure 10. Additionally, the reader is encouraged to watch the experiment in our YouTube video [60].

4.4. Key Insights from Comparing our Single-Integrator-Based and Unicycle-Based ESC Designs

In this subsection, we provide a brief comparison between the proposed unicycle-based ESC design and our single-integrator-based ESC design we presented in [12]. The comparison is based on two elements: convergence speed and design compactness/simplicity.

For the first element, convergence speed, we focus on two experimental cases, in both of which, TurtleBot3 (TB3) robot was employed under relatively similar conditions. For the first experimental case, we turn our attention to the source seeking experiment using a known objective function as reported in the single-integrator-based ESC design in [12] and the proposed unicycle-based ESC design in this work. The

robot started motion from the initial position $(2, 2)$. The single-integrator-based ESC design took approximately 40,000 seconds to reach the source position $(1, 1)$, with high oscillations observed throughout, as shown in [12, Figure 7, Section 3.B]. This behavior is also demonstrated in the corresponding YouTube video [61]. In contrast, the proposed unicycle-based ESC design achieved the same task, reaching the source location $(1, 1)$ and stopping at it, in *only* 350 seconds, as shown in Figure 8. The corresponding YouTube video showcasing this result can be accessed at [56]. For the second experimental case, we turn our attention to the model-free light source seeking experiment. The single-integrator-based ESC design required approximately 3,000 seconds to reach the light source, as shown in [12, Figure 9, Section 3.C], see our YouTube video in [62]. In comparison, the proposed unicycle-based ESC design accomplished the task in *just* 24 seconds, as illustrated in Figure 9. The corresponding YouTube video demonstrating this result can be found in [58]. These comparisons highlight the significant improvements in convergence speed achieved by the proposed design over our, very recently, proposed single-integrator-based ESC design [12].

For the second element, the compactness/simplicity of the design, it is crucial to emphasize that the proposed unicycle-based ESC design is a much more simple, compact and efficient design – with considerably less parameters to tune – compared to the single-integrator-based ESC design in [12]. That is, the proposed unicycle-based ESC design needs one simple ESC law of the form (1) for v and one adaptation law for a (see (15)) as opposed to two different ESC laws of the form (1) for x and y with two adaptation laws for a_x and a_y (see [12, Eq.(5)]). As a result, the proposed design is more efficient.

5. Concluding Remarks and Future Work

In this paper, we proposed a novel unicycle-based extremum seeking control (ESC) design, which can be applied as an effective mean for model-free, real-time source-seeking by robots (particularly differential wheeled robots). This approach is a bio-inspired approach given recent efforts that utilized extremum seeking methods to analyze/mimic optimized biological behaviors, including source-seeking – as in Figure 2. In summary, the proposed design is a very simple, model-free, real-time design that: (I) has no state integrators; (II) has attenuating oscillations, enabling the robot to stop at the source if it is fixed and follow the source if it is moving; (III) has improved convergence speed; and (IV) handles noise better. Moreover, all claimed advantageous, (I)-(IV), have been validated and verified via simulations, and more importantly, via real-world experiments. The proposed design outperformed the traditional unicycle ESC design found in literature and it also outperformed our, very recently, developed single-integrator-based ESC design in [12]. Building on the effectiveness of the proposed design, other source-seeking problems can be tested, including source-seeking with object avoidance, expanding the entire framework to 3D, and introducing a bio-inspired ESC design for flying robots (e.g., UAVs).

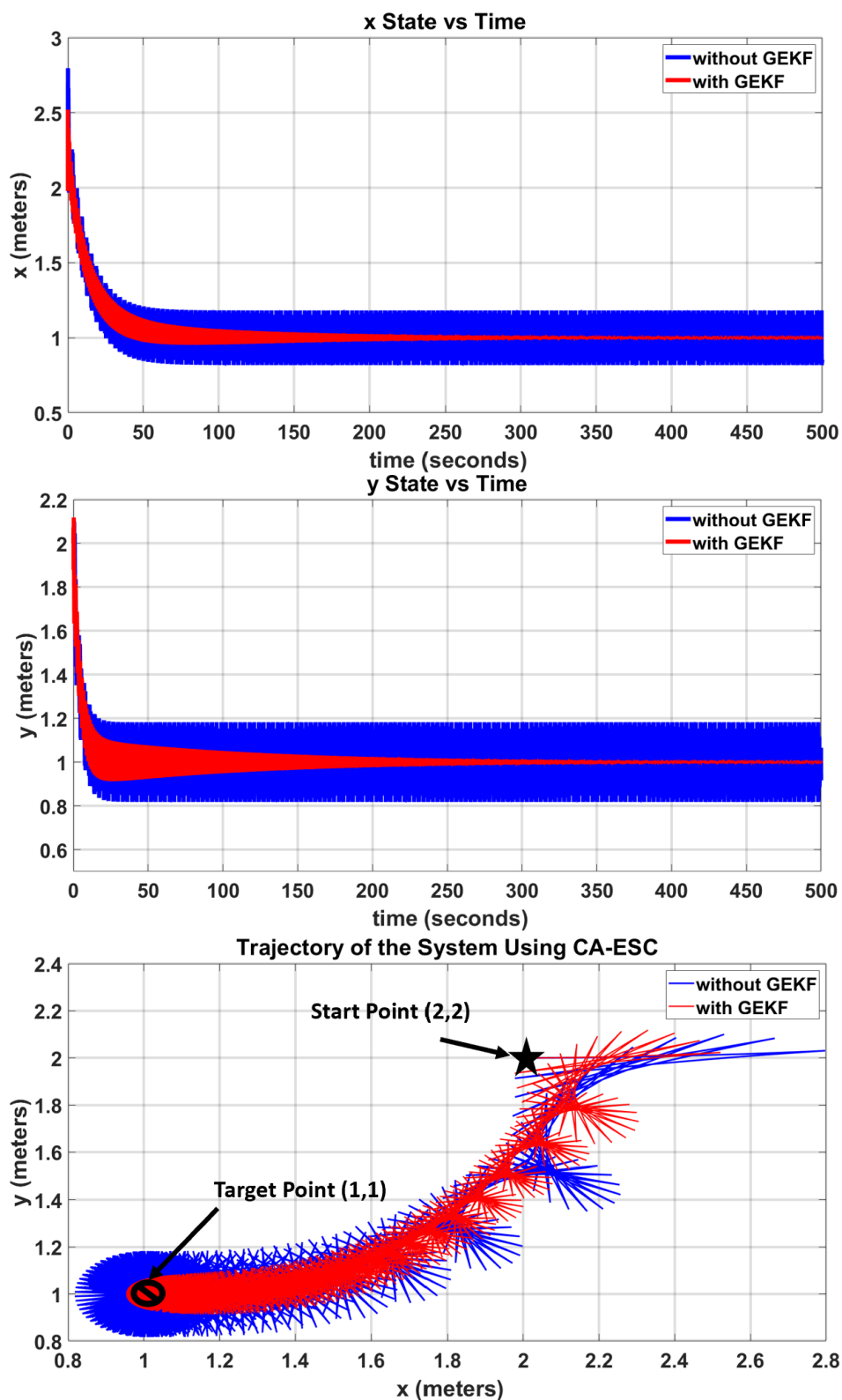


Figure 7: Simulation results for x - and y -coordinates and the planar trajectory, obtained using a known objective function. The proposed design (red) demonstrates successful attenuation of oscillations as apposed to the baseline design from the literature (blue).

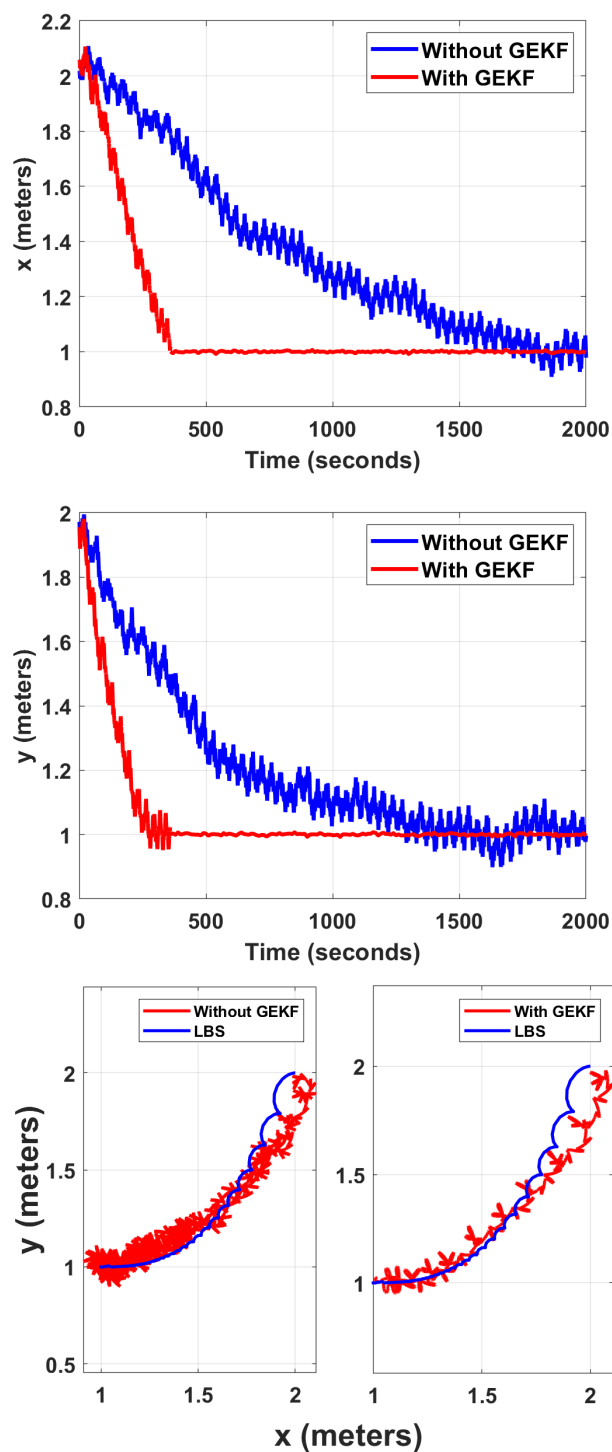


Figure 8: Trajectories of x - and y -coordinates captured using a motion capture system during real-world, real-time TB3 robotic experiments. The experiments were conducted twice to compare our proposed design (red) with the literature baseline design (blue). The results clearly demonstrate that our design attenuates oscillations, achieves faster convergence with shorter path, and effectively stops at the source position.

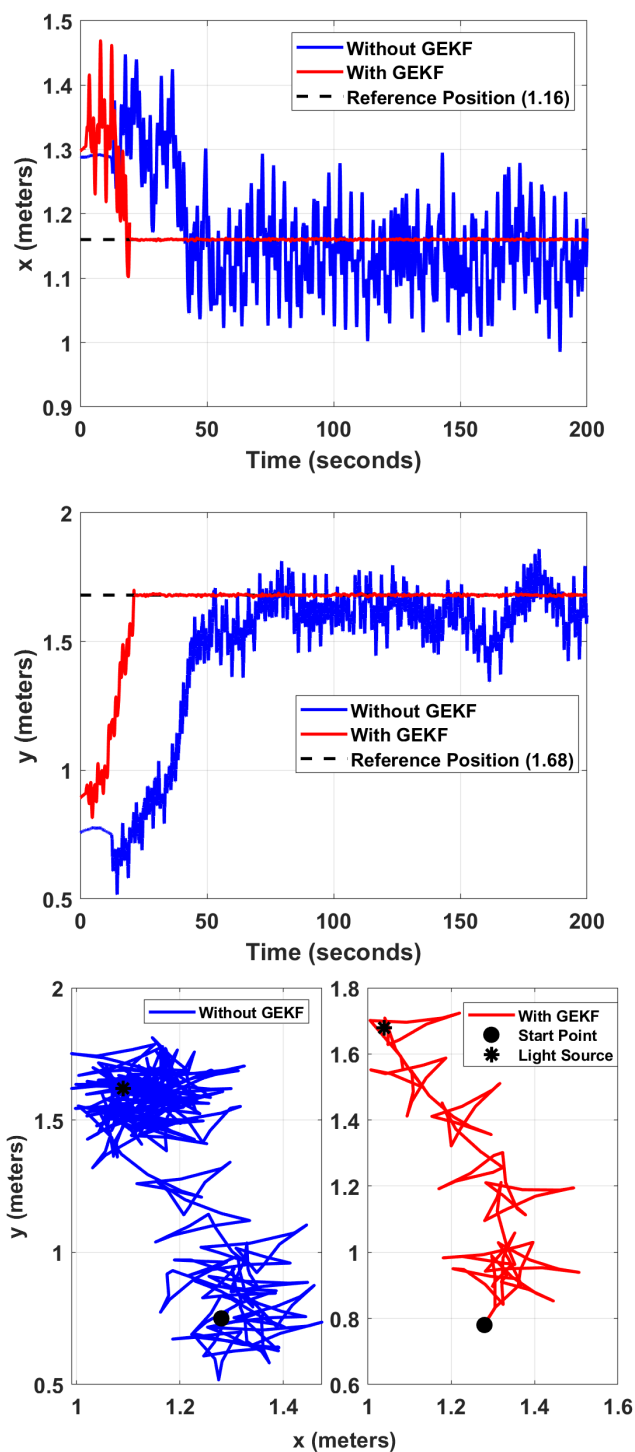


Figure 9: Trajectories of x - and y -coordinates captured via a motion capture system during real-world, real-time TB3 robotic experiments. The experiments measure light intensity using sensors. The experiments were conducted twice to compare our proposed design (red) with the baseline literature design (blue). The results clearly demonstrate that our design attenuates oscillations and achieves much faster convergence.

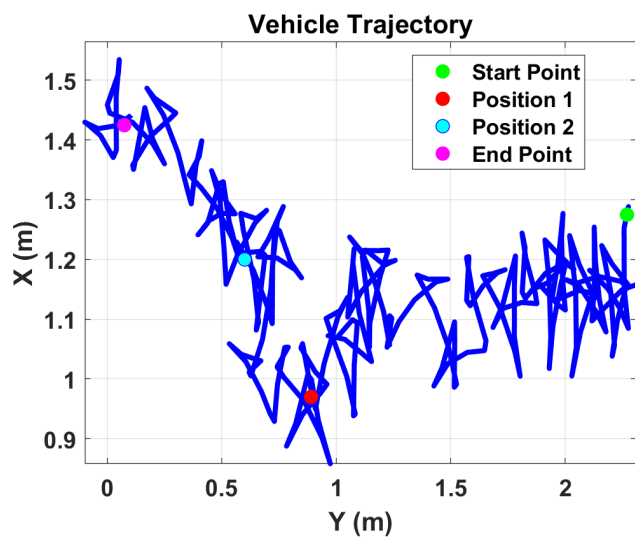


Figure 10: Planar trajectories captured by a motion capture system (MCS) of the TurtleBot3 (TB3) during moving light source-seeking experiment using our proposed design. The light source changes its position over time, and the TB3 was able to effectively track the moving light source.

References

- [1] M. Zhang, H. Wang, and J. Wu, “On uav source seeking with complex dynamic characteristics and multiple constraints: A cooperative standoff monitoring mode,” *Aerospace Science and Technology*, vol. 121, p. 107315, 2022.
- [2] W. Li, J. A. Farrell, S. Pang, and R. M. Arrieta, “Moth-inspired chemical plume tracing on an autonomous underwater vehicle,” *IEEE Transactions on Robotics*, vol. 22, no. 2, pp. 292–307, 2006.
- [3] R. Zou, V. Kalivarapu, E. Winer, J. Oliver, and S. Bhattacharya, “Particle swarm optimization-based source seeking,” *IEEE Transactions on Automation Science and Engineering*, vol. 12, no. 3, pp. 865–875, 2015.
- [4] K. Worthmann, M. W. Mehrez, M. Zanon, G. K. Mann, R. G. Gosine, and M. Diehl, “Model predictive control of nonholonomic mobile robots without stabilizing constraints and costs,” *IEEE transactions on control systems technology*, vol. 24, no. 4, pp. 1394–1406, 2015.
- [5] K. Worthmann, M. Mehrez, M. Zanon, G. K. Mann, R. G. Gosine, and M. Diehl, “Regulation of differential drive robots using continuous time mpc without stabilizing constraints or costs,” *IFAC-PapersOnLine*, vol. 48, no. 23, pp. 129–135, 2015.
- [6] K. D. Dimble, J. M. Faddy, and J. S. Humbert, “Electrolocation-based underwater obstacle avoidance using wide-field integration methods,” *Bioinspiration & biomimetics*, vol. 9, no. 1, p. 016012, 2014.
- [7] U. Zangina, S. Buyamin, M. S. Z. Abidin, M. S. Azimi, and H. Hasan, “Non-linear pid controller for trajectory tracking of a differential drive mobile robot,” *Journal of Mechanical Engineering Research and Developments*, vol. 43, no. 7, pp. 255–270, 2020.
- [8] J. Heikkinen, T. Minav, and A. D. Stotckaia, “Self-tuning parameter fuzzy pid controller for autonomous differential drive mobile robot,” in *2017 XX IEEE international conference on soft computing and measurements (SCM)*. IEEE, 2017, pp. 382–385.
- [9] D. Chwa, “Tracking control of differential-drive wheeled mobile robots using a backstepping-like feedback linearization,” *IEEE Transactions on Systems, Man, and Cybernetics-Part A: Systems and Humans*, vol. 40, no. 6, pp. 1285–1295, 2010.
- [10] J. Cochran, A. Siranosian, N. Ghods, and M. Krstic, “Gps denied source seeking for underactuated autonomous vehicles in 3d,” in *2008 IEEE International Conference on Robotics and Automation*. IEEE, 2008, pp. 2228–2233.
- [11] J. Cochran, E. Kanso, S. D. Kelly, H. Xiong, and M. Krstic, “Source seeking for two nonholonomic models of fish locomotion,” *IEEE Transactions on Robotics*, vol. 25, no. 5, pp. 1166–1176, 2009.
- [12] S. Bajpai, A. A. Elgohary, and S. A. Eisa, “Model-free source seeking by a novel single-integrator with attenuating oscillations and better convergence rate: Robotic experiments,” in *2024 European Control Conference (ECC)*. IEEE, 2024, pp. 472–479.
- [13] V. Grushkovskaya, S. Michalowsky, A. Zuyev, M. May, and C. Ebenbauer, “A family of extremum seeking laws for a unicycle model with a moving target: theoretical and experimental studies,” in *2018 European Control Conference (ECC)*. IEEE, 2018, pp. 1–6.
- [14] M. Abdelgalil, A. Eldesoukey, and H. Taha, “Singularly perturbed averaging with application to bio-inspired 3d source seeking,” in *2023 American Control Conference (ACC)*. IEEE, 2023, pp. 885–890.
- [15] S. Zhuo, “Source seeking of multi-uav based on extremum seeking algorithm,” in *2017 17th International Conference on Control, Automation and Systems (ICCAS)*. IEEE, 2017, pp. 1062–1067.
- [16] S. Pokhrel, A. A. Elgohary, and S. Eisa, “Extremum seeking by multi-agent vehicles and uavs with no steady state oscillation using a geometric-based kalman filtering,” in *AIAA SCITECH 2024 Forum*, 2024, p. 0724.
- [17] V. Todorovski and M. Krstic, “Newton nonholonomic source seeking for distance-dependent maps,” *IEEE Transactions on Automatic Control*, 2024.

- [18] A. S. Matveev, M. C. Hoy, and A. V. Savkin, “Extremum seeking navigation without derivative estimation of a mobile robot in a dynamic environmental field,” *IEEE Transactions on Control Systems Technology*, vol. 24, no. 3, pp. 1084–1091, 2015.
- [19] C. D. Hopkins, “A biological function for electroreception in sharks and rays,” *Journal of Experimental Biology*, vol. 213, no. 7, pp. 1005–1007, 2010.
- [20] R. W. Clark, G. S. Bakken, E. J. Reed, and A. Soni, “Pit viper thermography: the pit organ used by crotaline snakes to detect thermal contrast has poor spatial resolution,” *Journal of Experimental Biology*, vol. 225, no. 24, p. jeb244478, 2022.
- [21] C. Pennycuick, “Information systems for flying animals,” *Theoretical Ecology Series*, vol. 5, pp. 305–331, 2008.
- [22] V. Lebastard, F. Boyer, and S. Lanneau, “Reactive underwater object inspection based on artificial electric sense,” *Bioinspiration & Biomimetics*, vol. 11, no. 4, p. 045003, 2016.
- [23] I. Rañó, “A systematic analysis of the braitenberg vehicle 2b for point-like stimulus sources,” *Bioinspiration & biomimetics*, vol. 7, no. 3, p. 036015, 2012.
- [24] I. Rañó and J. A. Santos, “A biologically inspired controller to solve the coverage problem in robotics,” *Bioinspiration & biomimetics*, vol. 12, no. 3, p. 035002, 2017.
- [25] K. A. Daltorio, B. T. Mirlletz, A. Sterenstein, J. C. Cheng, A. Watson, M. Kesavan, J. A. Bender, J. Martin, R. E. Ritzmann, and R. D. Quinn, “How cockroaches exploit tactile boundaries to find new shelters,” *Bioinspiration & Biomimetics*, vol. 10, no. 6, p. 065002, 2015.
- [26] F. Boyer and M. Porez, “Multibody system dynamics for bio-inspired locomotion: from geometric structures to computational aspects,” *Bioinspiration & biomimetics*, vol. 10, no. 2, p. 025007, 2015.
- [27] D. Bierbach, L. Gómez-Nava, F. A. Francisco, J. Lukas, L. Musiolek, V. V. Hafner, T. Landgraf, P. Romanczuk, and J. Krause, “Live fish learn to anticipate the movement of a fish-like robot,” *Bioinspiration & Biomimetics*, vol. 17, no. 6, p. 065007, 2022.
- [28] A. Scheinker, “100 years of extremum seeking: A survey,” *Automatica*, vol. 161, p. 111481, 2024.
- [29] K. B. Ariyur and M. Krstic, *Real-time optimization by extremum-seeking control*. John Wiley & Sons, 2003.
- [30] A. Scheinker and M. Krstić, *Model-free stabilization by extremum seeking*. Springer, 2017.
- [31] S. Pokhrel and S. A. Eisa, “A novel hypothesis for how albatrosses optimize their flight physics in real-time: an extremum seeking model and control for dynamic soaring,” *Bioinspiration & Biomimetics*, vol. 18, no. 1, p. 016014, 2022.
- [32] S. A. Eisa and S. Pokhrel, “Analyzing and mimicking the optimized flight physics of soaring birds: A differential geometric control and extremum seeking system approach with real time implementation,” *SIAM Journal on Applied Mathematics*, pp. S82–S104, 2023.
- [33] A. A. Elgohary and S. A. Eisa, “Hovering flight in flapping insects and hummingbirds: A natural real-time and stable extremum seeking feedback system,” *arXiv preprint arXiv:2402.04985*, 2024.
- [34] B. Moidel, A. A. Elgohary, S. Bajpai, and S. Eisa, “Reintroducing the formation flight problem via extremum seeking control,” in *AIAA SCITECH 2024 Forum*, 2024, p. 2317.
- [35] M. Abdelgalil, Y. Aboelkassem, and H. Taha, “Sea urchin sperm exploit extremum seeking control to find the egg,” *Physical Review E*, vol. 106, no. 6, p. L062401, 2022.
- [36] M. Krstic and J. Cochran, “Extremum seeking for motion optimization: From bacteria to nonholonomic vehicles,” in *2008 Chinese Control and Decision Conference*. IEEE, 2008, pp. 18–27.
- [37] M. Krstic and H.-H. Wang, “Stability of extremum seeking feedback for general nonlinear dynamic systems,” *Automatica-Kidlington*, vol. 36, no. 4, pp. 595–602, 2000.
- [38] H.-B. Dürr, M. S. Stanković, C. Ebenbauer, and K. H. Johansson, “Lie bracket approximation of extremum seeking systems,” *Automatica*, vol. 49, no. 6, pp. 1538–1552, 2013.
- [39] S. Pokhrel and S. A. Eisa, “Higher order lie bracket approximation and averaging of control-affine systems with application to extremum seeking,” *provisionally accepted in Automatica (available as arXiv preprint arXiv:2310.07092)*, 2023.

- [40] N. Ghods, *Extremum seeking for mobile robots*. University of California, San Diego, 2011.
- [41] T. Xu, G. Chen, G. Zhou, Z. Liu, Z. Zhang, and S. Yuan, “Fast source seeking with obstacle avoidance via extremum seeking control,” in *2022 13th Asian Control Conference (ASCC)*. IEEE, 2022, pp. 2097–2102.
- [42] E. A. Bulgur, H. Demircioglu, and H. I. Basturk, “Light source tracking with quadrotor by using extremum seeking control,” in *2018 Annual American Control Conference (ACC)*. IEEE, 2018, pp. 1746–1751.
- [43] T. R. Oliveira, N. O. Aminde, and L. Hsu, “Monitoring function based extremum seeking control for uncertain relative degrees with light source seeking experiments,” in *53rd IEEE conference on decision and control*. IEEE, 2014, pp. 3456–3462.
- [44] S. Bajpai, “Investigating the performance of different controllers in optimized path tracking in robotics: A lie bracket system and extremum seeking approach,” Master’s thesis, University of Cincinnati, 2024.
- [45] ROBOTIS, “Turtlebot3 e-manual,” Online. [Online]. Available: <https://emanual.robotis.com/docs/en/platform/turtlebot3/overview/>
- [46] (2023) Light source seeking by the classic structure of extremum seeking control using angular velocity. [Online]. Available: <https://www.youtube.com/watch?v=9seWa-6tggU&t=1s>
- [47] A. Scheinker and M. Krstić, “Extremum seeking with bounded update rates,” *Systems & Control Letters*, vol. 63, pp. 25–31, 2014.
- [48] V. Grushkovskaya, A. Zuyev, and C. Ebenbauer, “On a class of generating vector fields for the extremum seeking problem: Lie bracket approximation and stability properties,” *Automatica*, vol. 94, pp. 151–160, 2018.
- [49] S. Pokhrel and S. A. Eisa, “Control-affine extremum seeking control with attenuating oscillations: A lie bracket estimation approach,” in *2023 Proceedings of the Conference on Control and its Applications (CT)*. SIAM, 2023, pp. 133–140.
- [50] —, “Gradient and lie bracket estimation of extremum seeking systems: A novel geometric-based kalman filter and relaxed time-dependent stability condition,” *International Journal of Control, Automation and Systems*, vol. 21, no. 12, pp. 3839–3849, 2023.
- [51] M. S. Stanković, H.-B. Dürr, and K. H. Johansson, “A lie bracket approximation for extremum seeking vehicles,” *IFAC Proceedings Volumes*, vol. 44, no. 1, pp. 11 393–11 398, 2011.
- [52] R. Suttner and S. Dashkovskiy, “Exponential stability for extremum seeking control systems,” *IFAC-PapersOnLine*, vol. 50, no. 1, pp. 15 464–15 470, 2017, 20th IFAC World Congress.
- [53] A. Scheinker and D. Scheinker, “Bounded extremum seeking with discontinuous dithers,” *Automatica*, vol. 69, pp. 250–257, 2016.
- [54] H.-B. Dürr, M. Krstić, A. Scheinker, and C. Ebenbauer, “Extremum seeking for dynamic maps using lie brackets and singular perturbations,” *Automatica*, vol. 83, pp. 91–99, 2017.
- [55] MDCL, “Modeling, dynamics and control lab,” Online. [Online]. Available: <https://sites.google.com/view/uc-aeem-mdcl/home>
- [56] (2025) Source seeking by robot: Unicycle-based extremum seeking with novel geometric-based kalman filtering. [Online]. Available: <https://www.youtube.com/watch?v=oWwD1DxtqaY>
- [57] (2025) Source seeking by robot : Unicycle extremum seeking approach. [Online]. Available: <https://www.youtube.com/watch?v=iEhqfHW7GuY>
- [58] (2025) Light source seeking: Unicycle-based extremum seeking with novel geometric-based kalman filtering. [Online]. Available: <https://www.youtube.com/watch?v=XjyPL75MY0o>
- [59] (2025) Light source seeking by robot : Unicycle extremum seeking control. [Online]. Available: <https://www.youtube.com/watch?v=nTSENhekKW0>
- [60] (2025) Source seeking for moving light source: Unicycle-based extremum seeking with gekf. [Online]. Available: https://www.youtube.com/watch?v=LmipEpx_2aU
- [61] (2023) Source seeking by geometric based kalman filtering with control affine extremum seeking. [Online]. Available: <https://www.youtube.com/watch?v=TLom8YMZojg>
- [62] (2023) Source seeking of light by novel extremum seeking design with attenuating

oscillation. [Online]. Available: https://www.youtube.com/watch?v=DTd_5bJpxVk, <https://www.youtube.com/watch?v=fM-2Qt3Zldg>

[63] A. Isidori, *Nonlinear control systems: an introduction*. Springer, 1985.

Appendix

Appendix .1. The Chen-Fliess Expansion (mentioned in Section 2.3)

Here we discuss briefly the Chen-Fliess functional expansion [63, Chapter 3]. The Chen-Fliess functional expansion provides a mathematical representation of the input-output behavior of a nonlinear system described by a control-affine differential equation such as (3) and an associated output function $y = h(\mathbf{x})$, where $y \in \mathbb{R}$. Consider a fixed time interval $[0, T]$ and real-valued, piecewise continuous functions u_1, \dots, u_m defined on this interval. For any multi-index (i_k, \dots, i_0) , the Chen-Fliess expansion provides the output $y(t)$ for a short time $t \in [0, T]$ as:

$$y(t) = h(\mathbf{x}_0) + \sum_{k=0}^{\infty} \sum_{i_0, \dots, i_k=0}^m L_{\mathbf{b}_{i_0}} \dots L_{\mathbf{b}_{i_k}} h(\mathbf{x}_0) \int_0^t d\xi_{i_k} \dots d\xi_{i_0}, \quad (.1)$$

where $L_{\mathbf{b}}h$ denotes the Lie derivative of h along \mathbf{b} , defined as $L_{\mathbf{b}}h = \nabla h \cdot \mathbf{b}$; and the iterated integral is expressed as:

$$\int_0^t d\xi_{i_k} \dots d\xi_{i_0} = \int_0^t d\xi_{i_k}(\tau) \int_0^{\tau} d\xi_{i_{k-1}} \dots \int_0^{\tau} d\xi_{i_0},$$

with $0 \leq t \leq T$, $\xi_0(t) = t$, and $\xi_i(t) = \int_0^t u_i(\tau) d\tau$ for $1 \leq i \leq m$.

Appendix .2. Derivation of The Lie-Bracket System Used in Section 4.1

Let us start with the first three equations in (15):

$$\begin{aligned} \dot{x} &= c(f(x, y) - eh) \cos(\Omega t) \sqrt{\omega} \sin(\omega t) + \cos(\Omega t) a \sqrt{\omega} \cos(\omega t) \\ \dot{y} &= c(f(x, y) - eh) \sin(\Omega t) \sqrt{\omega} \sin(\omega t) + \sin(\Omega t) a \sqrt{\omega} \cos(\omega t) \\ \dot{e} &= -he + f(x, y). \end{aligned} \quad (.2)$$

Now, we define the vector fields f and g as follows:

$$f = \begin{bmatrix} c(f(x, y) - eh) \cos(\Omega t) \\ c(f(x, y) - eh) \sin(\Omega t) \\ 0 \end{bmatrix},$$

$$g = \begin{bmatrix} a \cos(\Omega t) \\ a \sin(\Omega t) \\ 0 \end{bmatrix}.$$

By using [51, Lemma 1] and $\theta := \frac{t}{\epsilon} = \omega t$, we obtain for the following approximating system:

$$\begin{bmatrix} \dot{x} \\ \dot{y} \\ \dot{e} \end{bmatrix} = \begin{bmatrix} 0 \\ 0 \\ -\bar{e}h + f(x, y) \end{bmatrix} + \frac{1}{2\pi} \nu_{1,2}[f, g], \quad (.3)$$

where $\nu_{1,2}$ is defined as

$$\nu_{1,2} = \int_0^{2\pi} \int_0^\theta \sin(\tau) \cos(\theta) d\tau d\theta = -\pi.$$

Now, we compute the Lie bracket $[f, g]$ using the definition of Lie bracket between two vector fields:

$$[f, g] = \frac{\partial g}{\partial x} f - \frac{\partial f}{\partial x} g. \quad (.4)$$

That is,

$$\begin{aligned} [f, g] &= \begin{bmatrix} 0 & 0 & 0 \\ 0 & 0 & 0 \\ 0 & 0 & 0 \end{bmatrix} \begin{bmatrix} c(f(x, y) - eh) \cos(\Omega t) \\ c(f(x, y) - eh) \sin(\Omega t) \\ 0 \end{bmatrix} \\ &- \begin{bmatrix} c \cos(\Omega t) \cdot \nabla_x f(x, y) & c \cos(\Omega t) \cdot \nabla_y f(x, y) & -ch \cos(\Omega t) \\ c \sin(\Omega t) \cdot \nabla_x f(x, y) & c \sin(\Omega t) \cdot \nabla_y f(x, y) & -ch \sin(\Omega t) \\ 0 & 0 & 0 \end{bmatrix} \begin{bmatrix} a \cos(\Omega t) \\ a \sin(\Omega t) \\ 0 \end{bmatrix}. \end{aligned} \quad (.5)$$

We proceed by simplifying the above calculation:

$$[f, g] = - \begin{bmatrix} ca \cos^2(\Omega t) \cdot \nabla_x f(x, y) + ca \cos(\Omega t) \sin(\Omega t) \cdot \nabla_y f(x, y) \\ ca \sin(\Omega t) \cos(\Omega t) \cdot \nabla_x f(x, y) + ca \sin^2(\Omega t) \cdot \nabla_y f(x, y) \\ 0 \end{bmatrix}. \quad (.6)$$

By substituting (.6) into .3, we get the desired Lie-bracket system corresponding to the ESC system as follows:

$$\begin{bmatrix} \dot{x} \\ \dot{y} \\ \dot{e} \end{bmatrix} = \frac{1}{2} \begin{bmatrix} ca \nabla_x f(x, y) \cos^2(\Omega t) + ca \nabla_y f(x, y) \cos(\Omega t) \sin(\Omega t) \\ ca \nabla_y f(x, y) \sin^2(\Omega t) + ca \nabla_x f(x, y) \cos(\Omega t) \sin(\Omega t) \\ 2(-\bar{e}h + f(x, y)) \end{bmatrix}. \quad (.7)$$